

Artificial Neural Network evaluation of Poincaré constant for Voronoi polygons

Beatrice Crippa, Silvia Bertoluzza, Micol Pennacchio

Istituto di Matematica Applicata e Tecnologie Informatiche "E. Magenes" CNR, Pavia, Italy

Abstract. We propose a method, based on Artificial Neural Networks, that learns the dependence of the constant in the Poincaré inequality on polygonal elements of Voronoi meshes, on some geometrical metrics of the element. The cost of this kind of algorithms mainly resides in the data preprocessing and learning phases, that can be performed offline once and for all, constructing an efficient method for computing the constant, which is needed in the design of a posteriori error estimates in numerical mesh-based schemes for the solution of Partial Differential Equations.

Keywords. Poincaré constants; Artificial Neural Networks; Machine Learning; polygonal mesh

1. Introduction. The Poincaré inequality, which states that the H^1 semi norm of a zero mean function, multiplied by a positive real constant C_p , is an upper bound for its L^2 -norm, plays a key role in the design of a posteriori error analysis of many numerical schemes for the solution of Partial Differential Equations. In mesh-based numerical methods, such as Finite Elements or, more generally, polytopal elements such as Discontinuous Galerkin or Virtual Elements, the inequality is satisfied on each element of the tessellation for a suitable constant C_p depending on the element, and the design of reliable a posteriori error estimators would require the knowledge of such constant, which ideally enters in the definition of the error estimators. While an analytic expression for such a constant is not known in general, C_p can be determined through the solution of a PDE eigenvalue problem. Of course, solving such an eigenvalue problem for each element of a tessellation would be too expensive. In the framework of the two dimensional Finite Element method, where the elements are triangles, several works have then addressed the problem of providing estimates of such a constant as sharp as possible (see Section 2). When considering polygonal tessellations, the situation is clearly more complex. On the other hand, as the value of such a constant only depends on the geometry of the domain, we can try to put it in relation with some descriptive geometrical metrics.

To this aim, we can resort to Artificial Neural Networks (ANNs), a Machine Learning method that mimics the functioning of neural cells in the human brain, and that is recognized as powerful tool for the detection of relations between data inputs and numerical outputs. ANNs proved to be efficient in dealing with large quantities of data, and are usually applied to classification, pattern recognition, prediction and even function approximation. Indeed, they are able to learn the underlying (possibly nonlinear) relations between input and output data. In our case we believe that they can be trained to also learn how to approximate the Poincaré constant corresponding to a polytope, given some descriptive geometrical data. In this paper, we will apply an ANN-based model to the problem of finding C_p for convex polygons in \mathbb{R}^2 issued from Voronoi meshes, given some geometrical metrics of the polygon.

This paper has been realized in the framework of the MIUR Progetti di Ricerca di Rilevante Interesse Nazionale (PRIN) Bando 2017 (grant 201744KLJL) and of the ERC Project CHANGE, which has received funding from the European Research Council (ERC) under the European Union Horizon 2020 research and innovation programme (grant agreement n. 694515)

This method is much less computationally expensive than applying a finite element method to solve the eigenvalue problem on each element, as it only requires the solution of PDE eigenvalue problems in the training phase, that can be performed offline once and for all on a set of representative polygons. Once the model is properly defined and trained, determining the value of the constant on each element of a Voronoi mesh will be very fast.

In Section 2 we review the definition as well as some known results on the Poincaré constant and on its approximation. This will be followed by an overview of the structure and functioning of feed-forward dense ANNs in Section 3. Section 4 contains the method description, with the definition of the input attributes, details of the training set extraction from a Voronoi diagram, tuning method for the network hyperparameters and techniques for the optimization of the architecture and stabilization of the method. The experimental results are then reported in Section 5, while performance comparison of the different ANN models considered and the selection of the optimal one are discussed in Section 5.3. Some possible developments are presented in Section 6.

2. Known results on Poincaré constant. Letting $\Omega \subset \mathbb{R}^d$, $d \geq 2$, denote a bounded domain with Lipschitz boundary $\partial\Omega$, we consider a Poincaré-type inequality of the form:

$$\|w\|_{0,\Omega} \leq C_\Omega \|\nabla w\|_{0,\Omega}, \quad \forall w \in \tilde{H}^1(\Omega) := \left\{ w \in H^1(\Omega) : \int_\Omega w \, dx = 0 \right\}, \quad (1)$$

where

$$\|w\|_{0,\Omega}^2 = \int_\Omega |w|^2 \, dx.$$

It is well known that such an inequality holds for a constant C_Ω depending on Ω .

The Poincaré inequality plays a key role in the a posteriori analysis in many mesh-based Polytopal Element Methods (PEM [33]) for the solution of PDEs, such as Discontinuous Galerkin (DG [34]) and Virtual Element Methods (VEM [7, 6]), that rely on the construction of a partition T on the PDE domain, made of polytopes $\{E\}_{E \in T}$. In these cases, a posteriori error bounds are split into contributions of the individual mesh elements, weighted by with respective constants which depend, among other things, on the Poicaré constant for the element.

For a generic domain Ω , the analytic expression of the minimal constant C_Ω for which (1) holds is not known a priori, but it is associated with the minimal positive eigenvalue of the following problem :

Find $u \in \tilde{H}^1(\Omega)$, $\lambda \in \mathbb{R}$ such that

$$\begin{cases} -\Delta u = \lambda u & \text{in } \Omega, \\ \partial_{\mathbf{n}} u = 0 & \text{on } \partial\Omega. \end{cases} \quad (2)$$

This problem has a countable number of solutions $\{(u_i, \lambda_i)\}_i$, with $\lambda_i > 0$ for all i . Then, the sequence of eigenvalues can be ordered into a sequence $0 < \lambda_1 \leq \lambda_2 \leq \lambda_3 \leq \dots$, and the value of the Poincaré constant can be computed as follows:

$$C_\Omega^2 = \frac{1}{\lambda_1}. \quad (3)$$

As, to exploit this property in the design of a posteriori error estimator would require the solutions of problem (2) separately on each of element, which is of course too expensive, what is usually

done, is to look for sharp estimates of such a constant by investigating sharp bounds on the solution of (2). We recall that the dependence of the constant on the elements diameter is known in general, so that we only need to put it in an explicit relation with their shape. Simple bounds can be proved for convex polygons, generic triangles and isosceles triangles, and even the exact values for rectangles, cubes and right triangles are computed in [25] (because of the application to FEM, and therefore to triangular elements, most of the literature is focused on estimating the constant on triangles.). The first positive eigenvalue of problem (2) was roughly found by Lamé [18] and proved later in [24]. More in general, Matculevich and Repin [23] derived sharp two-sided bounds for triangular and tetrahedral domains.

Laugesen and Siudeja [19] proved an upper bound for a generic triangle T with diameter $d(T)$, defined as its longest edge:

$$C_T \leq \frac{d(T)}{j_{1,1}},$$

where $j_{1,1} = 3.83170597\dots$ is the first positive root of the Bessel functional J_1 [9].

The exact value of the constant for the right isosceles triangle with equal sides of length 1 is $C_{T_0} = \frac{1}{\pi}$. Kikuchi and Liu [15] proved that, given the amplitude θ of an interior angle and the measures α and β of the adjacent edges, an upper bound for C_p on T can be expressed as follows:

$$C_T \leq C_{T_0} \sqrt{1 + |\cos\theta|} \max\{\alpha, \beta\}.$$

A similar result is proved in [27] for any convex polygon P :

$$C_p \leq \frac{d(P)}{\pi},$$

where the diameter $d(P)$ is taken as the largest distance between two vertices. Many more bounds on the Poincaré constant on generic domains can be found in [29, 32], but up to now there is no proven shortcut for the determination in generic cases.

3. Artificial Neural Networks. A robust machine learning method, mainly applied to classification, pattern recognition and prediction in many disciplines consists in Artificial Neural Networks (ANNs).

ANNs are computational learning systems made of interconnected nodes, called neurons, and grouped into layers, that transform data inputs into numeric outputs, learning the relation between them in a preliminary training phase. Feed-forward dense neural networks are the most simple architectures and consist of one input layer containing the data, one output layer providing the result and some intermediate hidden layers and performing the actual approximation task. Each neuron takes as input a vector $\mathbf{x} = [x_1, x_2, \dots, x_N]^T$ of data, whose entries coincide with the output of all the neurons in the previous layer, and gives a single output. Their structure is schematized in Figure 1.

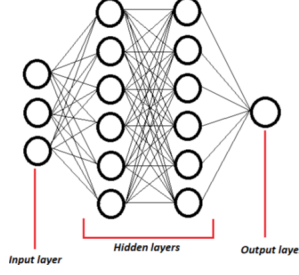


Figure 1. Structure of a feed-forward dense neural network with two hidden layers made of six neurons each. The input layer consists of the input data and the output layer gives the result. The middle layers are called hidden and are made of interconnected nodes, called neurons.

If we enumerate the neurons in each layer $l = 1, \dots, L$ from 1 to N_l , the output of neuron j in layer l is computed as the evaluation of a chosen real activation function σ at the weighted sum of the input with respect to specific parameters w_{jk}^l , $j = 1, \dots, N_l$, $k = 1, \dots, N_{l-1}$, $l = 1, \dots, L$, and a bias b_j^l , $l = 1, \dots, L$. A popular and simple choice of activation function is the rectified linear unit (ReLU), i.e. $\sigma(x) = x^+ = \max\{x, 0\}$.

Finally, the output of each neuron of the ANN can be expressed as follows:

$$a_j^l = \sigma \left(\sum_{k=1}^{N_{l-1}} w_{jk}^l a_k^{l-1} + b_j^l \right), \quad (4)$$

$\forall j = 1, \dots, N_l$, $l = 1, \dots, L$, where the parameters are set during the training phase. This stage consists in the minimization via gradient descent-based algorithms of a loss function, usually expressed as a sum of squared errors:

$$J(\mathbf{x}; W, \mathbf{b}) = \frac{\|\mathbf{y}^{\text{out}}(\mathbf{x}) - \mathbf{y}^{\text{true}}\|^2}{2N}, \quad (5)$$

where W is the collection of all the weights $\{w_{jk}^l\}_{jkl}$, $j = 1, \dots, N_l$, $k = 1, \dots, N_{l-1}$, $l = 1, \dots, L$, \mathbf{b} the vector of the biases $\{b_j^l\}_{jl}$, $j = 1, \dots, N_l$, $l = 1, \dots, L$, and $\|\cdot\|$ the Euclidean norm. The loss function of the output layer is given by (5), while in the hidden layers it is modified according to the backpropagation algorithm [20, 30]. An example of the structure of a feed-forward backpropagation ANN is presented in Figure 2. The goal of the backpropagation algorithm is to provide the set of parameters that gives the output minimizing (5). This procedure consists of two phases: a forward and a backward one. After an initialization of weights and biases, every unit determines its state according to equation (4), then optimization via gradient descent of the weights can be performed after the evaluation of the partial derivatives with respect to every parameter of the loss function (5) at each unit. The first part is called forward because for the state evaluation the neurons require the output of the ones in the previous layer, while the second is called backward because the expression of the partial derivatives can be derived for each unit as a function of the errors produced in the following layer.

The performance of an ANN depends on the design of its architecture, based on the tuning of the so-called hyperparameters, that may include the number of layers and neurons, the activation function, etc. There exist some automatic tuning methods and heuristics [12, 36] for the design of

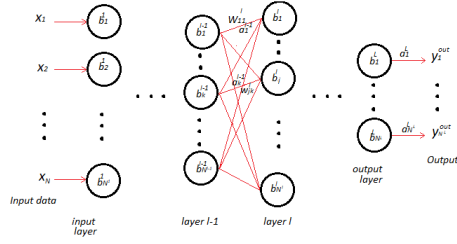


Figure 2. Scheme of a backpropagation network.

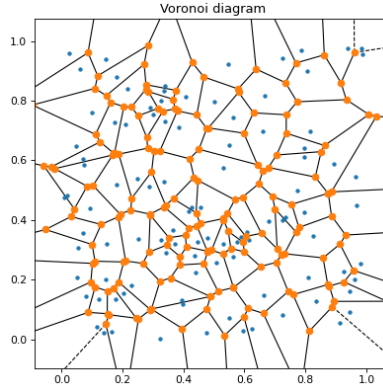


Figure 3. Voronoi diagram associated with $n = 100$ points (in blue) randomly sampled in $[0, 1]^2$ according to the uniform distribution. The regions delimited by vertices of the diagram (represented by orange points) are the considered Voronoi polygons.

the ANN structure, but the choice is often made by trial and error.

Another fundamental step in the definition of the model is the input variables selection: indeed, machine learning algorithms are used for discovering patterns among the attributes of many data, but some of them might be not as useful as others or even the high correlation between two attributes can make this task more difficult. A preliminary feature engineering phase can actually significantly improve the quality of the results and speed up the training process, and for further performance optimization other dimensionality reduction techniques, such as Principal Component Analysis can be applied without loss of accuracy [28, 4].

4. Method description. As explained in the previous sections, we are interested in the estimation of the Poincaré constant in inequality (1), that is only dependent on the shape of the domain of definition. Since ANNs are able to uncover relations between data features and numerical outputs, in the following section we introduce an ANN-based method for the solution of this problem, where the data given as input to the Machine Learning model are a set of geometrical features related to the input and the output is an approximation of the associated constant.

We restrict the study to 2-dimensional convex polygons. For the training dataset generation, we consider the finite regions of a Voronoi diagram [21, 3] associated with n randomly sampled points in a subset of \mathbb{R}^2 , as shown in Figure 3.

Attene *et al.* [1] analyzed the impact of a list of geometrical features of the underlying mesh on the performance of VEM and concluded that it is not driven by any one singularly, even though

some of them seem to have a more central role than others. The attributes considered as input for the ANN model described below are the same properties considered in their work, defined on every polygon P as follows:

- **Circumscribed circle radius (CC)**, i.e. the radius of the smallest circle entirely containing P , computed applying Welzl’s algorithm [37] to its vertices;
- **Inscribed circle radius (IC)**, i.e. radius of the largest circle contained in P , determined as the largest circle centered in a vertex of the Voronoi skeleton of P [26];
- **Circle ratio (CR)**: $CR = \frac{IC}{CC} \in [0, 1]$;
- **Area (AR)**;
- **Kernel area (KE)**, i.e. the area of the set of points $p \in P$ from which the polygon is visible, determined as the intersection of the half-planes generated by the edges if P is not convex and coincident with P otherwise;
- **Kernel-area ratio (KAR)**: $KAR = \frac{KE}{AR} \in [0, 1]$;
- **Area-perimeter squared ratio (APR)**: $APR = \frac{AR}{\text{perimeter}^2} \in [0, 1]$;
- **Shortest edge (SE)**;
- **Scaled shortest edge (sSE)**: $sSE = \frac{SE}{CC} \in [0, 1]$;
- **Edge ratio (ER)**: $ER = \frac{SE}{\text{longest edge}} \in [0, 1]$;
- **Minimum point-to-point distance (MPD)**, i.e. the minimum distance between two vertices;
- **Scaled minimum point-to-point distance (sMPD)**: $sMPD = \frac{MPD}{CC} \in [0, 1]$;
- **Minimum (inner) angle (MA)**;
- **Maximum (inner) angle (MX)**;
- **Shape regularity (SR)**: $SR = \frac{\text{radius of the circle inscribed in the kernel}}{CC} \in [0, 1]$;
- **Isotropy (ISO)**, i.e. the ratio between the minimum and maximum eigenvalue of the covariance matrix $M_{cov} := \frac{1}{AR} \int_P (x - \bar{x}_P)^T (x - \bar{x}_P) dx$, where \bar{x}_P denotes the barycenter of P .

However, some of the listed features are redundant when referred to convex polygons, whose kernel coincides with the polygon itself. As a consequence, we can discard the kernel area (equivalent to the area), the kernel-area ratio (equal to 1) and the shape regularity (equivalent to the circle ratio).

Moreover, in Section 5 a further dimensionality reduction is performed, based on the elimination of highly correlated variables.

The considered attributes are given as input to a feed-forward dense neural network with L hidden layers, made of N neurons each, using ReLU activation function. Each neuron in the

input layer corresponds to a different geometrical feature of a polygon, computed during the pre-processing phase, and is connected to each unit in the first layer. Instead, the output layer consists of a single linear unit, providing the final result, i.e. the estimate of the corresponding Poincaré constant. The network parameters $\{w_{jk}^l\}_{jkl}$ and $\{b_j^l\}_{jl}$, with $j = 1, \dots, N_l$, $k = 1, \dots, N_{l-1}$, $l = 1, \dots, L$, are learned during the training process by minimization of the loss function (5), where the target value \mathbf{y}^{true} is given as the inverse of the minimum eigenvalue of problem (2), determined via second order FEM. The employed optimization algorithm is Adam [16], with learning rate initially fixed as $\eta = 10^{-3}$ and then tuned in order to analyze its influence on the performance of the ANN.

The whole implementation of the ANN-based method relies on the Python library TensorFlow [11] and the hyperparameters N and L are tuned in two stages: a first observation of the differences in the evaluation of the loss function on a validation set, taken as 30% of the training data, followed by an automatic search based on Keras Bayesian Optimization [5] on a limited set of efficient values.

4.1. STRUCTURE OPTIMIZATION STRATEGIES. Fully-connected layers are the most intuitive Neural Network architecture, but many improvements can be introduced by modifications of the optimal dense structure. Indeed, after reducing the dimensionality of the input variables and tuning the optimal hyperparameters, we can additionally stabilize the model and speed up the training phase by eliminating some connections. One strategy is to set to 0 the weights corresponding to the units whose inclusion or exclusion affects the global error the least (pruning), while another consists in the omission of random neurons with fixed probability p during training, as if the final model is an average of all the possible networks (dropout).

Oversized ANNs can cause overfitting of the training data and consequently present poor generalization ability. In order to overcome the risk of noise tuning and introduce sparsity, smaller networks can be obtained by trimming the deeper ones through the elimination of some connections between units in increasing order of sensitivity of the total error to their exclusion. The pruning procedure does not interfere with the learning process and implies a negligible computational overload.

Many pruning techniques can be applied [14, 2], but we will only exploit the magnitude-based ones, that consist in sorting the weights on each pruning step with respect to their magnitude and delete the smallest ones until the desired sparsity level is reached. We consider the sparsity to be polynomially decaying throughout the training phase, starting at iteration t_0 and performing a pruning step every Δt (both t_0 and Δt are parameters to be tuned), updating the sparsity as follows:

$$s_t = s_f + (s_0 - s_f) \left(1 - \frac{t - t_0}{n_{pr} \Delta t} \right),$$

$\forall t = 0, \dots, n_{pr} \Delta t$, where n_{pr} indicates the number of total pruning iterations, s_f the target final sparsity and s_0 the initial one. The effectiveness of this method, also implemented in the Python TensorFlow Model Optimization toolkit [35], in reducing the training computational cost and memory footprint is investigated in [38], where a comparison between a small dense network and a larger sparse one is also performed. The authors observed that, at memory requirement parity, the second one provides higher accuracy. Therefore, in the next section the results obtained by a large sparse network are also presented.

Finally, we will also analyze a fully-connected network where some of the neurons in the original architecture are completely eliminated. This structure is selected by applying the same Bayesian

Optimization search used for tuning the hyperparameters, allowing a non-homogeneous number of neurons per layer, lower than the previous one.

The last stabilization applied is dropout, i.e. a stochastic technique based on random modifications of the network parameters only during training. This approach should help avoiding overfitting and improving the generalization error, as showed in [10]. Indeed, ReLU activation is faster than sigmoid ones but also more prone to overfit the data.

The dropout output of a hidden layer during the training phase is given by the following expression:

$$\mathbf{y} = \sigma(W\mathbf{x} + \mathbf{b}) \circ \mathbf{m}, \quad m_i \stackrel{\text{iid}}{\sim} Be(1 - p),$$

where the vector \mathbf{m} is called dropout mask and all of its components are independent random variables with Bernoulli distribution, taking value 1 with probability $1 - p$ and 0 with probability p . The dropout mask is used to set to 0 random components of the output. The output of the trained model is instead given as the average of all possible network structures:

$$\mathbf{y} = (1 - p)\sigma(W\mathbf{x} + \mathbf{b}).$$

This is the standard dropout method, based on the random elimination of some connections and proposed by Hinton *et al.* [13], but many other implementations exist (see [17]).

5. Results. As anticipated in the previous section, the tests are performed on convex polygons generated by the Voronoi diagram of $n = 100$ randomly sampled points in $[0, 1]^2$ according to the uniform distribution. The geometrical features were computed relying on the Python package *scikit-geometry* [31], while the approximation of the Poincaré constant as the solution of problem (2) makes use of the *FEniCS* package [22]. The constant computation is made by applying second order FEM on a mesh with elements diameter equal to $\frac{1}{20}$ of the polygon diameter.

The first step of the model selection consists in dimensionality reduction according to the correlation between variables. The correlation values are reported in Table 1, where we can observe that the highest ones are registered between MA and MX, CR, APR and ISO and SE, sSE and ER. Moreover, the correlations between SE and MPD and their scaled counterparts are exactly 1, and this can be due to the fact that in the considered sample the minimum distance between two vertices always coincides with the shortest edge.

High correlation means that one attribute can be expressed as a function of the other, and indeed in the scatterplots represented in Figure 4 we can clearly observe the relations between them. As a consequence, only one attribute for each of these sets is kept: MX, since it was proved to have a key role also in the VEM performance in [1], ISO, since both CR and APR are obtained as a function of other variables (IC, CC and AR), and ER, because it is the most descriptive in its group, taking into account both SE and the longest edge measure.

Finally, the chosen attributes given as input to the ANN are the following: IC, CC, APR, ER, MX and ISO. An additional regularization step was to eliminate the outliers from the randomly generated training set, considered as all the samples with at least one attribute having z-score, i.e. distance, measured as number of standard deviations, from the population mean, ≥ 2 . Figure 5 shows the boxplots of the attributes in the training set, before and after the outliers elimination.

After the features engineering phase, we can go on and design the Neural Network structure. As anticipated in the previous section, we consider a feed-forward dense ANN, with ReLU activation function on all the hidden units, divided in groups of N neurons on L layers, and a linear output layer made of one neuron.

	IC	CC	CR	AR	APR	SE	sSE	ER	MPD	sMPD	MA	MX	ISO
IC	1	0.6377	0.4652	0.8121	0.4313	0.0020	-0.02362	-0.1615	0.0020	-0.02362	-0.1236	-0.0740	0.394
CC	-	1	-0.3125	0.9244	-0.3152	0.0554	-0.2291	-0.2084	0.0554	-0.2291	-0.1516	-0.0915	-0.2475
CR	-	-	1	0.0057	0.9095	-0.0737	0.0025	0.0680	-0.0737	0.0025	0.0606	0.0621	0.8561
AR	-	-	-	1	0.0134	0.0456	-0.2109	-0.1711	0.0456	-0.2109	-0.1200	-0.0529	0.0119
APR	-	-	-	-	1	-0.0358	0.0285	0.1170	-0.0358	0.0285	0.0503	0.0572	0.6789
SE	-	-	-	-	-	1	0.9171	0.9072	1	0.9171	-0.0603	-0.0595	0.0313
sSE	-	-	-	-	-	-	1	0.9698	0.9171	1	0.0086	-0.0050	0.0995
ER	-	-	-	-	-	-	-	1	0.9072	0.9698	-1.3255	-0.0098	0.1482
MPD	-	-	-	-	-	-	-	-	1	0.9171	-0.0603	-0.0595	0.0313
sMPD	-	-	-	-	-	-	-	-	-	1	0.0086	-0.0050	0.0995
MA	-	-	-	-	-	-	-	-	-	-	1	0.9832	0.0406
MX	-	-	-	-	-	-	-	-	-	-	-	1	0.0405
ISO	-	-	-	-	-	-	-	-	-	-	-	-	1

Table 1. Correlation between input attributes. We consider highly correlated the couples of variables with corresponding value ≥ 0.8 , like the groups $\{SE, sSE, ER, MA, MX\}$, $\{CR, AR, ISO\}$ and $\{MA, MX\}$.

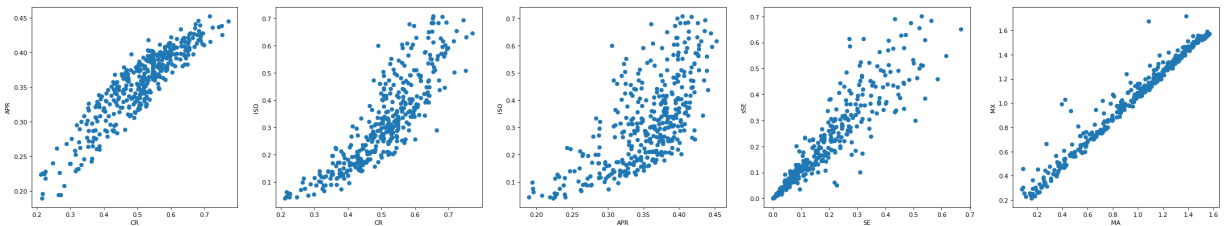
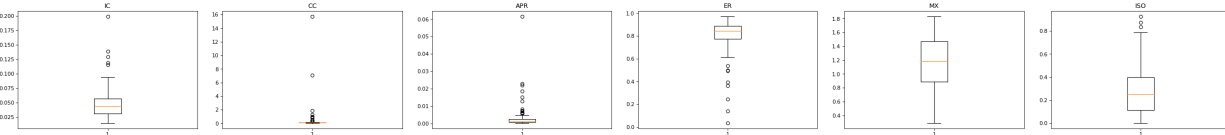
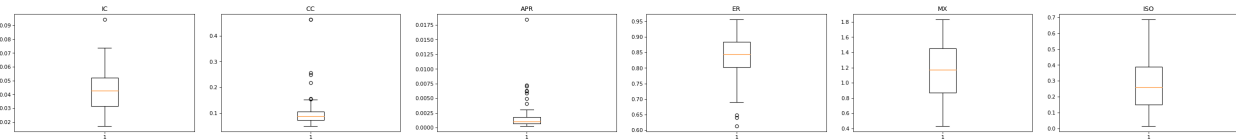


Figure 4. Scatterplots of correlated variables.



(a) Boxplots of the input attributes of the full training set.



(b) Boxplots of the input attributes of the dataset obtained by eliminating the outliers from the training set.

Figure 5. Comparison of the boxplots of the reduced dataset before (Figure 5a) and after (Figure 5b) the outliers elimination.

The hyperparameters we need to tune are N , L and the learning rate η of the optimization method. We will compare the network performance in correspondence of different combinations of these values. In particular, we divide the generated dataset D into a training set T and a validation set V , such that $D = T \cup V$ and $T \cap V = \emptyset$, taken as 70% and 30% of the data in D , respectively. The model will be trained on T and at the same time validated by evaluating the loss function (5) on V at each training epoch. The comparison among different network structure will be based on

the validation loss, defined as follows:

$$J_{\text{val}}(\mathbf{X}; W, \mathbf{b}) := \frac{\sum_{i=1}^{|\mathbf{V}|} J(\mathbf{x}_i; W, \mathbf{b})}{|\mathbf{V}|},$$

where $|\mathbf{V}|$ indicates the cardinality of \mathbf{V} and \mathbf{X} is the collection of all the validation data $\mathbf{x} \in \mathbf{V}$. We will finally analyze also the error made in the estimation of the constant on a separate set of polygons Voronoi corresponding to 65 random locations in $[0, 0.5]^2$, by evaluating the loss function (5).

Let us fix $\eta = 10^{-3}$ and observe the consequences of varying the values of L and N first. Figure 6 represents the validation loss over 200 training iterations when fixing the value of L and varying $N \in \{8, 32, 64, 128, 256, 512, 1024\}$. We can observe that higher N leads to faster decrease to the convergence value, but can also produce oscillations, indicating an unstable method. The instabilities are moreover amplified by a high number of hidden layers, while the minimum loss reached remains almost unchanged and of order 10^{-5} . In particular, oscillations are most accentuated when $N \geq 512$ or $L \geq 4$ and the method is very slow when $L = 1$ and $N \leq 128$. Therefore, the Bayesian Optimization search can be performed among the values $L \in \{2, 3\}$ and $N \in \{250, 251, \dots, 500\}$. Then, the optimal hyperparameters determined after 200 iterations of the algorithm over 200 training epochs result $L = 3$ and $N = 385$. Even if theoretically a deeper network could learn faster and improve the minimum validation loss obtained, we can see in Figure 7a that, for a fixed value of N , a too high number of layers results in worse performance, probability due to overfitting the small quantity of training data by estimating a too high number of unknown parameters. Something similar happens when increasing the number of hidden units, while keeping L fixed (Figure 7b), even if in this case the variation is not drastic in the order of magnitude. We can try to overcome this limitation and design a deeper neural network by increasing the training set dimension at the cost of greatest computational time, but from Figure 7c we can observe that for $N_{\text{train}} > 100$ the minimum validation loss achieved by a network with 3 fully connected hidden layers having 385 neurons each increases and the optimal training dataset seems to correspond to $N_{\text{train}} = 100$.

We can finally tune the learning rate value η . Let us fix $L = 3$ and $N = 385$ and observe the behavior of this network trained on the dataset corresponding to $N_{\text{train}} = 100$, for $\eta \in \{10^{-4}, 10^{-3}, 10^{-2}, 10^{-1}\}$ during 500 training iterations. Figure 8 shows that for $\eta = 0.1$ the method becomes very unstable and it gains the best stability for $\eta = 0.0001$. Moreover, even if the smallest learning rate makes the convergence slow and presents slightly higher validation loss in the first iterations, it converges to the lowest value. The highest values of validation loss are, however, reached by $\eta = 0.1$, where the plot seems to converge in almost 100 iterations to a local optimum, after initial wide oscillations up to 10^2 . Both in stability and in order of magnitude of the final validation loss there is no huge difference between $\eta = 0.001$ and $\eta = 0.0001$, but the slowdown introduced by the smallest learning rate is not significant and anyway it ends up in a smaller final error. Therefore, we can conclude that the best learning rate corresponds to $\eta = 0.0001$.

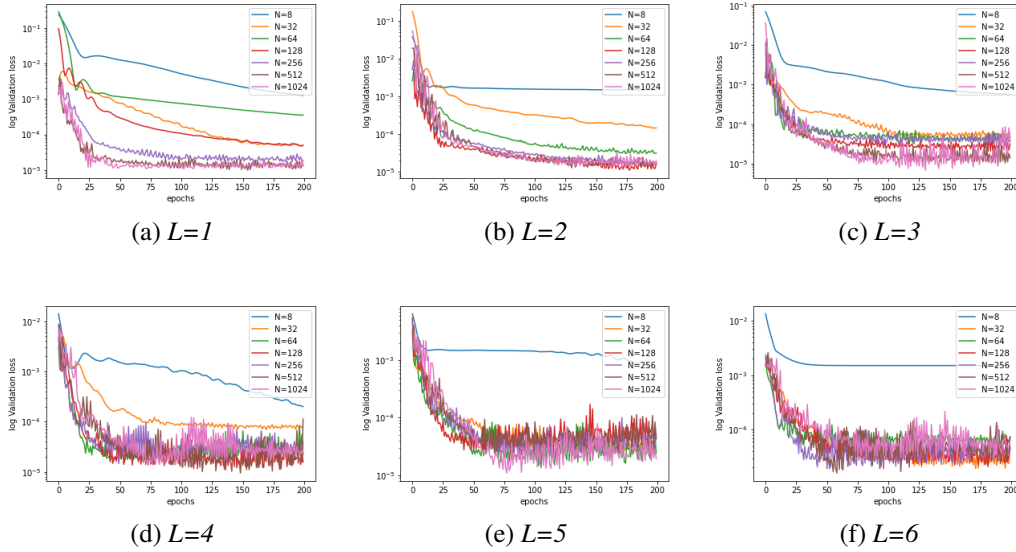


Figure 6. Loss function evaluated on the validation set at each of the 100 training epochs, for different values of $N \in \{8, 32, 64, 128, 256, 512, 1024\}$.

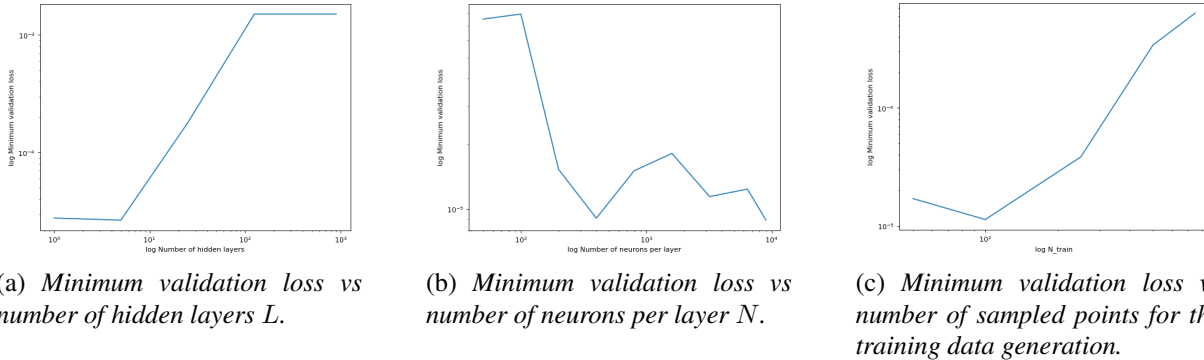


Figure 7. Logarithmic plots of the minimum validation loss with respect to the values of some hyperparameters. Figure 7a refers to the number of hidden layers and shows a sudden increase in the loss value in order of magnitude from 10^{-5} to 10^{-2} . Figure 7b considers the number of hidden units and shows a decreasing trend until $N = 300$, after which the graph starts to increase again. In Figure 7c N_{train} indicates the number of sampled points for the training data generation; the validation set is taken as the 30% of the generated dataset, that is defined as the geometry metrics computed for the Voronoi polygons in the diagram corresponding to N_{train} points in $\left[0, \left(\frac{N_{train}}{100}\right)^2\right]^2$.

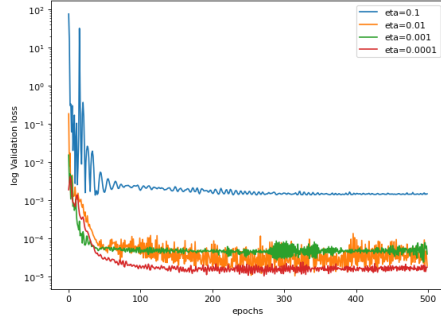
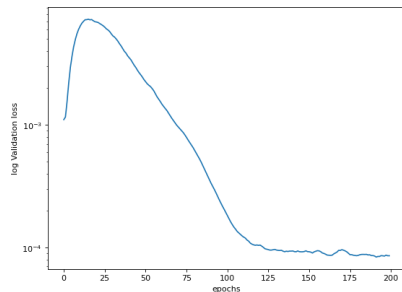


Figure 8. Semi-logarithmic plot of the validation loss during the first 100 training epochs for different values of η .

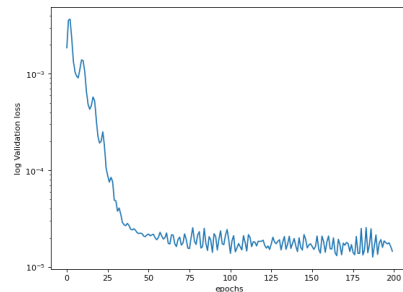
If we repeat the same process on the non-pre-processed dataset, we find out that the best feed-forward dense ANN model is made of 3 hidden layers with 76 neurons each and learning rate 10^{-4} . The performance of this model are, as expected, much worse than what obtained for pre-processed data. Indeed, the validation loss does not decrease below values of order 10^{-4} and presents an initial fast increase, followed by a slow descent to the convergence value. With the reduced dataset we obtain, instead, a decreasing loss that reaches in much less iterations a final value with one order of magnitude less than the previous case. See Figure 9 for the comparison between the validation loss obtained by the two models.

We can observe that

5.1. PRUNING. Once we have found the best feed-forward dense model, we can focus on the ANN with $L = 3$, $N = 385$ and taking as input the reduced dataset, and try to optimize the structure by eliminating some connections (i.e. setting some weights to 0) in order to speed up the evaluation phase.



(a) Network with 3 hidden layers, having 76 neurons each, taking as input the full dataset before preprocessing.



(b) Network with 3 hidden layers, having 385 neurons each, taking as input the pre-processed dataset with a reduced number of attributes and no outliers.

Figure 9. Comparison of the semi-logarithmic plots of the validation loss during the first 200 training epochs produced by the ANN model taking as input the full (Figure 9a) and reduced (Figure 9b) datasets.

First we select non-homogeneous numbers of neurons on each hidden layer, applying again

the Bayesian Optimization search algorithm with fixed number of hidden layers $L = 3$ and $N_i \leq 385 \quad \forall i = 1, \dots, L$. The best architecture obtained after 100 maximum trials has the following hyperparameters values: $N_1 = 326$, $N_2 = 324$, $N_3 = 70$. This network has 130656 total connections, equivalent to the 43.62% of the original one, with $7N + (L - 1)N^2 + N = 299530$ weights and in particular the first two hidden layers still have almost as many units as the original network, while the last one is much smaller.

Figure 10 shows the validation loss during the first 200 training iterations, with a very similar behavior as the plot corresponding to the dense model (Figure 9b).

We can now apply the pruning algorithm described in [38], starting at the t_0^{th} training iteration. Since it should start after a good level of convergence is achieved, according to Figure 9b we can choose $t_0 \geq 75$ and, in order to achieve faster convergence, couple this stabilization scheme with a higher learning rate $\eta = 10^{-3}$.

Figure 11 shows the validation loss during the first 200 training epochs, starting at $t_0 = 75$ and different levels of final sparsity p . All the plots present a peak after almost 50 iterations, after which the validation loss continues its decreasing trend, and whose amplitude depends on the choice of the hyperparameter p . Figure 12 shows the validation and test loss values obtained with different sparsity levels, and they are all around the same value, in particular validation loss at the last training epoch between $8 \cdot 10^{-6}$ and $2 \cdot 10^{-5}$, and test loss of order 10^{-4} . As well as the result of the optimal dense network with non-homogeneous number of neurons per layer, also in this case the best validation and test result are obtained for $p = 0.6$, and in particular the optimal parameters according to the Bayesian Optimization search algorithm for the automatic tuning of $p \in [0.5, 0.7]$ and $t_0 \in \{75, \dots, 125\}$ are $p = 0.67$, $t_0 = 78$.

Since a deeper network can learn higher-level relations among the input variables but at the same time too many tunable parameters can lead to overfitting the training data, we can apply pruning to an ANN with more hidden layers than the chosen optimal one. We expect to obtain a deeper model that also has good generalization ability, the same memory footprint as the smaller dense one and better accuracy.

In order to do so, we fix the number of neurons per layer as $\tilde{N} = N$ and choose the quantity of hidden layers \tilde{L} so that, after performing a pruning with final sparsity s_f it has as many connections as the small dense one:

$$7\tilde{N} + (\tilde{L} - 1)\tilde{N}^2 + \tilde{N} = \frac{7N + (L - 1)N^2 + N}{1 - s_f}.$$

If we set the sparsity as the optimal value chosen for the pruned network $s_f = 0.67$, then the missing hyperparameter shall be fixed to $\tilde{L} = 7$.

Figure 13 shows the comparison of the validation loss obtained in 200 training epochs by this model and the original smaller dense network, which have different sparsity level but same complexity. The sparse network is found by applying pruning with polynomially decreasing sparsity, starting from the 78^{th} training iteration and learning rate $\eta = 10^{-3}$, as these resulted to be the optimal choices in the previous pruning analysis.

The sparse ANN presents an initially fast decrease and a peak in the validation loss plot after 50 iterations, but then it starts to decrease again and reaches the lower values than the dense one.

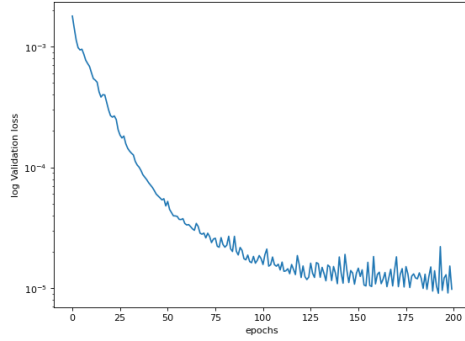


Figure 10. Semi-logarithmic plot of the validation loss during the first 200 training epochs of the network with 3 hidden layers, with different numbers of neurons per layer N_i , $i = 1, 2, 3$. In particular, $N_1 = 326$, $N_2 = 324$, $N_3 = 70$.

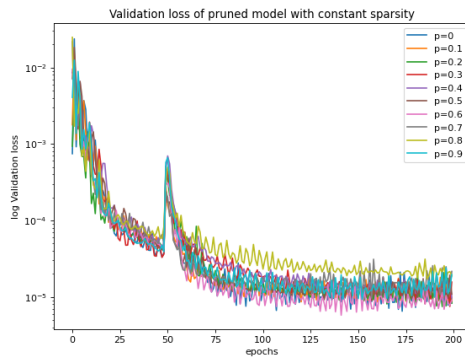


Figure 11. Semi-logarithmic plot of the validation loss during the first 200 training epochs of the pruned networks with polynomially decaying rate and final sparsity $p \in \{0, 0.1, 0.2, 0.3, 0.4, 0.5, 0.6, 0.7, 0.8, 0.9\}$, starting at $t_0 = 75$.

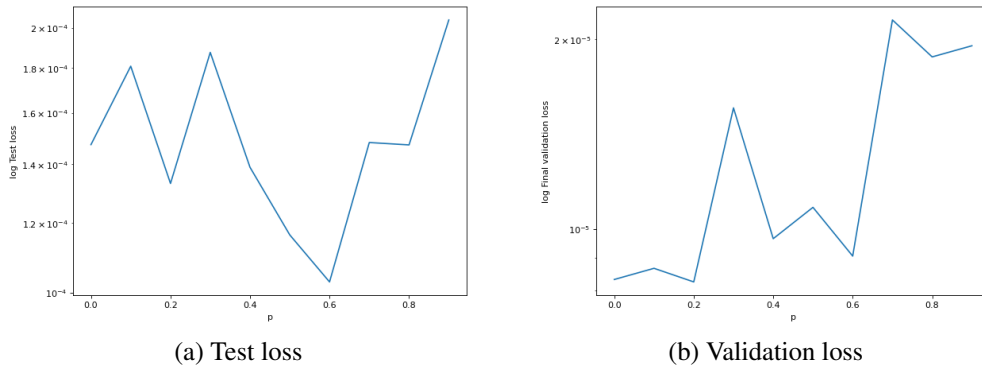


Figure 12. Semi-logarithmic plot of the validation and test loss obtained after 200 training epochs by the pruned networks with polynomially decaying sparsity, with respect to the final level p , starting at $t_0 = 75$.

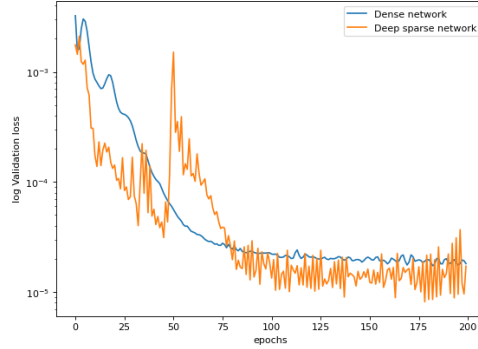


Figure 13. Semi-logarithmic plot of the validation loss of networks with different levels of sparsity and same number of connections $N_c = 299530$. The blue graph corresponds to a dense ANN with $L = 3$ hidden layers and $N = 385$ neurons each, while the orange one corresponds to an ANN with sparsity $s_f = 0.67$, the same value for N and $L = 7$.

5.2. DROPOUT. After tuning all the hyperparameters and analyzing the effect of changing the size of the input dataset on the method performance, we ended up with a model having $7N + N + (L - 1)(N^2 + N) + N + 1 = 300686$ total tunable parameters and a training set made of less than 100 polygons. As a consequence, the risk of overfitting the data is high and we can try to overcome it by applying the dropout method, consisting in introducing random modifications of the ANN during the learning process, and in particular we will discard every connection in between neurons in the hidden layers with probability p and between units in the input layer and on the first hidden one with probability $\frac{p}{4}$.

As we can see in Figure 14, even for small values of p , i.e. for insignificant modifications of the structure, the validation loss has much greater values and presents wider oscillations than when dropout is not introduced ($p = 0$). This happens because at every training epoch a different set of weights is optimized, and the result can only be observed in the test error (Figure 15), that is reduced for $p \in [0.1, 0.3]$ and reaches its minimum for $p = 0.3$, but increases a lot when $p \geq 0.4$.

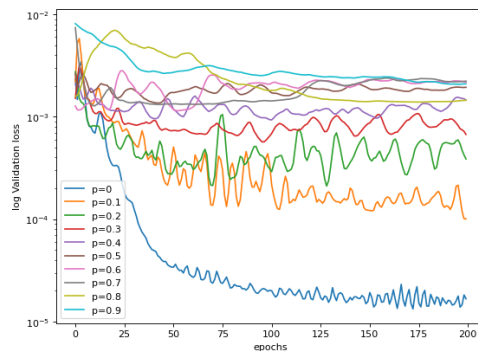


Figure 14. Validation loss during the first 200 training epochs of the network with dropout on all the hidden layers with probability $p \in \{0, 0.1, 0.2, 0.3, 0.4, 0.5, 0.6, 0.7, 0.8, 0.9\}$ and on the input layer with probability $\frac{p}{4}$.

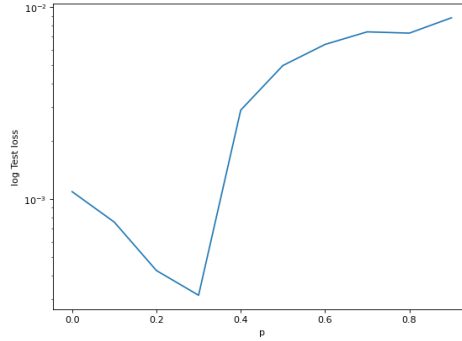


Figure 15. Semi-logarithmic plot of the test loss obtained after 200 training epochs of the network with respect to the dropout probability on the input layers.

Model	Minimum validation loss	Best epoch	Test loss	Training time	Test time
Full ANN	$2.0865 \cdot 10^{-5}$	490	$1.5885 \cdot 10^{-3}$	8.1812 s	0.0265 s
30% dropout	$5.6329 \cdot 10^{-4}$	268	$2.4151 \cdot 10^{-4}$	8.3071 s	0.0262 s
Non-homogeneous N	$2.0818 \cdot 10^{-5}$	414	$1.0131 \cdot 10^{-3}$	7.6100 s	0.0260 s
Deep sparse ANN	$1.2414 \cdot 10^{-5}$	121	$1.0816 \cdot 10^{-5}$	13.7785 s	0.0315 s
67% pruned ANN	$1.1848 \cdot 10^{-5}$	310	$5.5503 \cdot 10^{-6}$	9.7090 s	0.0286 s

Table 2. Performance comparison of all the considered models, trained for 500 epochs. The best epoch indicates the training iteration corresponding to the minimum value of validation loss.

5.3. PERFORMANCE COMPARISON. Table 2 summarizes the performance of all the considered models by analyzing the minimum value of validation loss reached, the number of training epochs needed, the test loss and the training and test time¹. In Figure 16 we can instead observe the behavior of the validation loss during the first 500 training epochs.

The deep sparse ANN converges in a small number of iterations and reaches the minimum validation loss in the least number of steps, but it is the slowest both at training and evaluation (the first is almost two times longer than any the fastest method). The second fastest model achieving its minimum validation loss is the 30% dropout ANN, but this value is the highest of all, of order 10^{-4} .

All the other methods are very similar both in terms of minimum loss and best epoch. However, the smallest validation loss is achieved by the 67% pruned network, that also presents narrow oscillations and the fastest decrease, despite a peak around the 50th training epoch. Moreover, the corresponding plot shows convergence after 100 iterations, implying the possibility of an early stopping of the training without loss in performance, that could help prevent overfitting the training data.

Finally, this model results stable and reliable, with the smallest test error, of order 10^{-6} , that improves the one obtained by the full ANN by 10^{-3} times. The training phase, that is the slowest and most computationally expensive part of the machine learning algorithms is actually pretty fast, as we can read from Table 2, while the test part takes almost the same time as the full ANN. Even if

¹ Time, measured in seconds, taken by a computer with Intel Core i9-10910 CPU (3.60GHz), 128GB RAM, macOS 11.6.6 running Python 3.9.7.

the test time is almost the same for every method, the fastest evaluation of the constant corresponds to the dense network with non-homogeneous number of neurons per layer, but provides a worse error, of order 10^{-3} . All the methods provide, however, very fast evaluations, compared to the FEM solution of the system (2), that takes almost 4.7070 seconds on our test set.

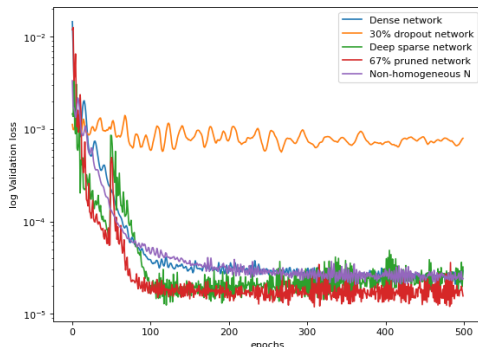


Figure 16. Semi-logarithmic plot of the validation loss of all the considered models, trained for 500 epochs.

6. Conclusions and further developments. We have defined a method for the estimation of the Poincaré constant on generic Voronoi polygons, based on Neural Networks taking as input some geometric metrics.

The value of the loss function on the validation set converges in a few hundreds of iterations during the training phase and the error is in principle at least of order 10^{-3} but can be reduced to 10^{-6} by introducing sparsity in the dense structure. Since the optimal ANN is not very deep and the constant evaluation after the training phase (that can be performed offline once and for all) consists of simple operations, such as multiplications and sums, the online part of the method is very fast.

Moreover, the required size of the input dataset is small and this implies little time spent also for its generation and preprocessing.

The downsides of this approach consist in the apparent impossibility of the error reduction below 10^{-6} in less than 500 iterations. Moreover, the absence of a solid theoretical background does not allow a simple definition of error bounds with respect to the ANN size.

We are currently trying to improve the idea presented in this paper by changing the variables given as input to the Artificial Neural Network. The first idea is to directly consider the Cartesian coordinates of the input vertices and add some convolutional layers in order to make the model translation- and rotation-independent. The same regularization can also be performed by defining an intrinsic polar coordinates system in every polygon, that can be passed to a dense ANN, that should result in lower computational time, despite a little longer preprocessing phase.

Another improvement can be introduced by rescaling all the polygons, so that they all have diameter=1 and their size does not create an issue for the generalization ability of the model.

In order to give an explanation of the error value, an a posteriori analysis of the influence of the approximation error in the FEM computation of Poincaré constants used for training on the final estimation error can be useful. Indeed, not only the FEM error is strictly related to the mesh granularity, and this could help us defining some error bounds on the final method, but also the noise in unreliable labels is much more harmful than incorrect or redundant attributes ([8, 39]) and

being able to somehow quantify it can help the model improvement.

Finally, the method will be tested on Adaptive FEM and then extended to other constants involved in polytopal schemes that depend only on the elements shape, like the trace inequality constant on stabilized methods (VEM, SUPG for Stokes problem).

Bibliography.

- [1] M. Attene, S. Biasotti, S. Bertoluzza, D. Cabiddu, M. Livesu, G. Patanè, M. Pennacchio, D. Prada, and M. Spagnuolo, “Benchmarking the geometrical robustness of a virtual element poisson solver,” *Mathematics and Computers in Simulation*, vol. 190, pp. 1392–1414, 2021.
- [2] M. G. Augasta and T. Kathirvalavakumar, “Pruning algorithms of neural networks — a comparative study,” *Open Computer Science*, vol. 3, no. 3, pp. 105–115, 2013.
- [3] F. Aurenhammer, “Voronoi diagrams—a survey of a fundamental geometric data structure,” *ACM Computing Surveys*, vol. 23, no. 3, 1991.
- [4] A. Azadeh, M. Sheikhalishahi, and M. Tabesh, “The effects of pre-processing methods on forecasting improvement of artificial neural networks,” *Australian Journal of Basic and Applied Sciences*, vol. 5, no. 6, pp. 570–580, 2011.
- [5] *BayesianOptimization Tuner*, Accessed: 2022-02-17. [Online]. Available: https://keras.io/api/keras_tuner/tuners/bayesian/.
- [6] L. Beirao Da Veiga, C. Canuto, R. Nochetto, G. Vacca, and M. Verani, “Adaptive vem: Stabilization-free a posteriori error analysis,” *arXiv*, 2021.
- [7] L. Beirao Da Veiga, L. Brezzi, A. Cangiani, G. Manzini, G. Marini, and A. Russo, “Basic principles of Virtual Element Methods,” *Mathematical Models and Methods in Applied Sciences*, vol. 23, no. 01, pp. 199–214, 2013.
- [8] A. J. Bekker and J. Goldberger, “Training deep neural-networks based on unreliable labels,” in *2016 IEEE International Conference on Acoustics, Speech and Signal Processing (ICASSP)*, 2016, pp. 2682–2686.
- [9] F. Bowman, *Introduction to Bessel functions*. Courier Corporation, 2012.
- [10] G. E. Dahl, T. N. Sainath, and G. E. Hinton, “Improving deep neural networks for LVCSR using rectified linear units and dropout,” in *2013 IEEE International Conference on Acoustics, Speech and Signal Processing*, 2013, pp. 8609–8613.
- [11] F. Ertam and G. Aydın, “Data classification with deep learning using Tensorflow,” in *2017 International Conference on Computer Science and Engineering (UBMK)*, 2017, pp. 755–758. DOI: [10.1109/UBMK.2017.8093521](https://doi.org/10.1109/UBMK.2017.8093521).
- [12] M. Feurer and F. Hutter, “Hyperparameter optimization,” in *Automated machine learning*, Springer, Cham, 2019, pp. 3–33.
- [13] G. E. Hinton, N. Srivastava, A. Krizhevsky, I. Sutskever, and R. R. Salakhutdinov, “Improving neural networks by preventing co-adaptation of feature detectors,” *arXiv*, 2012.
- [14] E. Karnin, “A simple procedure for pruning back-propagation trained neural networks,” *IEEE Transactions on Neural Networks*, vol. 1, no. 2, pp. 239–242, 1990.

- [15] F. Kikuchi and X. Liu, “Estimation of interpolation error constants for the p0 and p1 triangular finite elements,” *Computer Methods in Applied Mechanics and Engineering*, vol. 196, no. 37, pp. 3750–3758, 2007.
- [16] D. P. Kingma and J. Ba, *Adam: A method for stochastic optimization*, 2014.
- [17] A. Labach, H. Salehinejad, and S. Valaee, “Survey of Dropout Methods for Deep Neural Networks,” *arXiv*, 2019.
- [18] G. Lamé, *Leçons sur la théorie mathématique de l’élasticité des corps solides*. Bachelier, 1852.
- [19] R. Laugesen and B. Siudeja, “Minimizing Neumann fundamental tones of triangles: An optimal Poincaré inequality,” *Journal of Differential Equations*, vol. 249, no. 1, pp. 118–135, 2010.
- [20] Y. Lecun, “A theoretical framework for back-propagation,” in *Proceedings of the 1988 Connectionist Models Summer School, CMU, Pittsburg, PA*, D. Touretzky, G. Hinton, and T. Sejnowski, Eds., Morgan Kaufmann, 1988, pp. 21–28.
- [21] D. T. Lee and F. P. Preparata, “Computational geometry—a survey,” *IEEE Transactions on Computers*, vol. C-33, no. 12, pp. 1072–1101, 1984.
- [22] A. Logg, K. A. Mardalan, and G. Wells, *Automated Solution of Differential Equations by the Finite Element Method, The FEniCS book*. Springer, Berlin, Heidelberg, 2012.
- [23] S. Matculevich and S. Repin, “Sharp bounds of constants in poincare type inequalities for polygonal domains,” *arXiv*, 2015.
- [24] B. J. McCartin, “Eigenstructure of the equilateral triangle, part ii: The neumann problem,” *Mathematical Problems in Engineering*, vol. 8, no. 6, pp. 517–539, 2002.
- [25] A. I. Nazarov and S. I. Repin, “Exact constants in Poincaré type inequalities for functions with zero mean boundary traces,” *Mathematical Methods in the Applied Sciences*, vol. 38, no. 15, pp. 3195–3207, 2015.
- [26] R. L. Ogniewicz and M. Ilg, “Voronoi skeletons: Theory and applications.,” in *CVPR*, vol. 92, 1992, pp. 63–69.
- [27] L. E. Payne and H. F. Weinberger, “An optimal Poincaré inequality for convex domains,” *Archive for Rational Mechanics and Analysis*, vol. 5, pp. 286–292, 1960.
- [28] G. T. Reddy, M. P. K. Reddy, K. Lakshmana, R. Kaluri, D. S. Rajput, G. Srivastava, and T. Baker, “Analysis of dimensionality reduction techniques on big data,” *IEEE Access*, vol. 8, pp. 54 776–54 788, 2020.
- [29] S. Repin, “Computable majorants of constants in the Poincaré and Friedrichs inequalities.,” *Journal of Mathematical Sciences*, vol. 186, no. 2, 2012.
- [30] D. E. Rumelhart, G. E. Hinton, and R. J. Williams, “Learning representations by back-propagating errors,” *Nature*, vol. 323, pp. 533–536, 1986.
- [31] *Scikit-geometry documentation*, Accessed: 2022-02-09. [Online]. Available: <https://scikit-geometry.github.io/scikit-geometry/>.

- [32] I. Sebestova and T. Vejchodskyy, “Two-sided bounds for eigenvalues of differential operators with applications to Friedrichs, Poincaré, trace, and similar constants,” *SIAM Journal on Numerical Analysis*, vol. 52, no. 1, pp. 308–329, 2014.
- [33] N. Sukumar and A. Tabarraei, “Conforming polygonal finite elements,” *International Journal for Numerical Methods in Engineering*, vol. 61, no. 12, pp. 2045–2066, 2004.
- [34] L. R. S. Susanne C. Brenner, *The Mathematical Theory of Finite Element Methods*. Springer New York, NY, vol. 15.
- [35] *Tensorflow model optimization toolkit*, Accessed: 2022-03-22. [Online]. Available: https://www.tensorflow.org/model_optimization.
- [36] S. Walczak and N. Cerpa, “Heuristic principles for the design of artificial neural networks,” *Information and Software Technology*, vol. 41, no. 2, pp. 107–117, 1999.
- [37] E. Welzl, “Smallest enclosing disks (balls and ellipsoids),” in *New Results and New Trends in Computer Science*, H. Maurer, Ed., Springer Berlin Heidelberg, 1991, pp. 359–370.
- [38] M. Zhu and S. Gupta, “To prune, or not to prune: exploring the efficacy of pruning for model compression,” *arXiv*, 2017.
- [39] X. Zhu and X. Wu, “Class noise vs. attribute noise: A quantitative study,” *Artificial Intelligence Review*, vol. 22, pp. 177–210, 2004.